Int J Pept Res Ther (2015) 21:205–221
DOI 10.1007/s10989-014-9447-3

A Detailed Investigation on Conformation, Permeability and PK Properties of Two Related Cyclohexapeptides

Ian Lewis · Michael Schaefer · Trixie Wagner · Lukas Oberer · Emine Sager · Peter Wipfli · Thomas Vorherr

Accepted: 3 December 2014 / Published online: 23 December 2014

Abstract This contribution provides detailed insights regarding permeability properties of published cyclohexapeptides related to their conformation. The study includes data on oral bioavailability and PK parameters including application of a known enhancer. Interestingly, the latter did not show an effect, neither on the cyclic peptide exhibiting low oral uptake nor on the similar molecule showing a 30 % oral bioavailability in mice. These results are discussed in the context of exposed polar surface area for the preferred conformation and structural data obtained by NMR and X-ray crystallography.

Keywords Permeability · Pharmacokinetics · Cyclohexapeptides · Conformation

Abbreviations

Boc	Tert-butyloxylcarbonyl
BAV	Bioavailability on p.o. administration
CH_3CN	Acetonitrile
CL	In-vitro or in vivo clearance
CsA	Cyslosporine A
DCM	Dichloromethane
DIEA	DIPEA diisopropyl ethylamine
DMF	Dimethyl formamide
DDM	Dodecylmaltoside enhancer
LiOtBu	Lithium *t*-butoxide
NOESY	Nuclear Overhauser effect spectroscopy
PAMPA	Parallel artificial membrane permeability assay
MDCK	Madin Darby canine kidney cells
PPB	Plasma–protein binding
rmsd	Root mean squared deviation
p.o.	Per os
Rh	Hydrodynamic radius
ROESY	NOE in the rotating frame
RPHPLC	Reversed-phase high performance liquid chromatography
SAPSA	Solvent-accessible polar surface area
SFC	Supercritical fluid chromatography
TFA	Trifluoroacetic acid
TLC	Thin layer chromatography

Standard abbreviations for amino acids and peptide derivatives are according to the suggestion of the IUPAC-IUB Joint commission on Biochemistry Nomenclature: Eur. J. Biochem. 138 (1984) 9–37.

Electronic supplementary material The online version of this article (doi:10.1007/s10989-014-9447-3) contains supplementary material, which is available to authorized users.

I. Lewis (✉) · M. Schaefer · T. Wagner · L. Oberer · E. Sager · P. Wipfli · T. Vorherr
Novartis Institutes for Biomedical Research, 4002 Basel, Switzerland
e-mail: ian.lewis@novartis.com

Introduction

The interest in understanding and predicting the properties of cyclic peptides enabling cell permeability has recently been summarized from our perspective (Marzinzik and Vorherr 2013). There are three reasons justifying this increased attention. The first reason is the emergence of exciting new powerful screening technologies enabling the identification of macrocyclic peptide starting points already with exceptionally high binding affinities (Kenichiro et al. 2013). The second reason relates to the importance of intracellular targets in the oncology therapeutic area, where peptides may have significant advantages over small molecule approaches (Miranda et al. 2013). The third reason is the resurgence in the interest in therapeutic peptides for

oral applications where novel delivery technologies have increased opportunities for clinical intervention with this particular class (Mönkärea et al. 2012). Starting points for peptide medicinal chemistry have traditionally been natural products or naturally occurring hormones. Interesting examples include CsA (Chatterjee et al. 2008), Maurocalcine (Poillot et al. 2012) and Sanguinamide (Nielsen et al. 2012). On the other hand, synthetic, designed macrocycles have recently been pivotal in enlightening investigators concerning key features enhancing permeability properties. Indeed an understanding of comparatively simpler macrocycles may be a prerequisite to gain a fuller understanding of more complex permeable macrocyclic peptides such as CsA (Bockus 2013; Rezai et al. 2006, 2011; Rand et al. 2012). In the group of Horst Kessler, smaller cyclic peptides have been studied intensively to investigate features responsible for oral uptake (Chatterjee et al. 2008). Similarly, following in silico considerations, studies by Scott Lokey suggested two compounds for further analyses due to their pronounced difference for oral uptake, although the molecules are distinct only in 3 N-methyl groups (Rezai et al. 2011). This latter study, in particular the result of a 28 % oral bioavailability in rats for a tri-N-methylated cyclohexapeptide, prompted our interests to investigate further aiming at a more detailed understanding of the features responsible for transport.

Methods

Synthesis

Cyclic peptides (1) [Leu-D-Leu–Leu-Leu-D-Pro-Tyr] and (2) [Leu-NMe-D-Leu-NMe-Leu-Leu-D-Pro-NMe-Tyr] were synthesized starting with the allyl ester of fluorenylmethyloxycarbonyl (Fmoc)-protected tyrosine linked to a trityl polystyrene resin (TentaGel S Trt Cl from RAPP Polymere GmbH) similar to published procedures (Rezai et al. 2006; Chan and White 2000). For automated syntheses, peptides were prepared using a Symphony automated peptide synthesizer, subsequently cyclized and then cleaved from the resin. Amino acids, reagents and solvents were purchased from Bachem or Aldrich.

Solid Phase Synthesis of Cyclohexapeptide (2) Via Cyclohexapeptide (1)

Coupling 1 (Fmoc-D-Pro-OH onto Fmoc-Tyr-*O*-Allyl-Trityl resin): Fmoc deprotection was performed by stirring with 20 % 4-methylpiperidine in DMF (2 × 50 mL × 5 min) + (1 × 50 mL × 10 min). The resin was then washed with DMF (5×) and NMP (2×). To a solution of Fmoc-D-proline (0.640 g, 1.896 mmol) and PyOxim (1 g, 1.896 mmol) in DMF (15 mL)/NMP (15 mL), DIPEA (0.67 mL, 3.84 mmol) was added and the reaction mixture stirred for 2 min. The Kaiser test was used as a qualitative test for the presence or absence of free primary amino groups, indicating the completeness of a coupling step. The test is based on the reaction of ninhydrin with free primary amines, which gives a characteristic dark blue colour. This mixture was added to the resin and the suspension stirred for 45 min at RT (Kaiser test negative). The resin was filtered and washed with DMF (3×). Coupling and deprotection of other constituent amino acids was carried out similarly. Allyl ester deprotection procedure: The resin (0.599 g, 0.479 mmol) was swollen with 0.3 % DIPEA in DCM × 15 min and washed with THF and filtered. $Pd(PPh_3)_4$ (0.055 g, 0.048 mmol) and 10 % Piperidine in THF (25 mL) were added and the suspension shaked for 2 h at rt. Workup: The resin was filtered and washed with 5 % sodium diethyldithiocarbamate in 5 % DIPEA/DMF (2× 25 mL), DMF (5×), NMP(3×) and 0.3 % DIPEA in DCM (2×). On resin cyclization procedure: The resin (2.7 g, 0404 mmol) was swollen with 0.3 % DIPEA in DCM for 15 min and washed with DMF 2×. A premixed solution of HATU (0.461 g, 1.212 mmol), HOAt (0.165 g, 1.212 mmol) and DIPEA (0.423 mL, 2.424 mmol) in DMF (15 mL)/NMP (15.00 mL) was added to the resin and the suspension shaken at rt for 18 h. Workup: The resin was filtered and washed with 5 % sodium diethyldithiocarbamate in 5 % DIPEA/DMF (2 × 25 mL), DMF (5×), NMP(3×) and 0.3 % DIPEA in DCM (2×). On resin N-methylation procedure: The resin (0.5 g, 0.516 mmol) was swollen in 1 % DIPEA in DCM for 15 min, washed with THF 2× and filtered. A solution of lithium *t*-butoxide 1 M in THF (10 mL, 10.00 mmol) was added and the resin shaken for 30 min at RT. The resin was filtered and without washing, a solution of MeI, 10 % in DMSO (10 mL, 0.516 mmol) was then added and the resin shaked for a further 30 min. The resin was filtered and washed with DMF 2×, H_2O 2×, DMF 3× and DCM. The peptide was cleaved from the resin using 10 % TFA in DCM 4 × 5 min × 5 mL and washed with DCM 3× 5 mL. The cleavage solution and the DCM washes were collected and the solvent evaporated under reduced pressure to give a yellow oil. Purification was carried out by prep-RP-HPLC utilizing solvent A: Water 0.1 % TFA Solvent B: Acetonitrile combined with a 2487 Waters UV detector at 224 nm and a 30 × 150 mm Atlantis Prep T3 OBD 5 µm preparative column. The fractions of interest were pooled and lyophilized to give the desired product as a white powder.

High-Throughput Equilibrium Solubility

Sample preparation for high-throughput equilibrium solubility determination is performed in microtiter plate format

on an automated platform that is based on a STARPlus module (Hamilton). In addition, the platform comprises a centrifuge (Rotanta, Hettich), two plate-shakers (TiMix 5, Edmund Bühler), a heat sealer (ALPS-3000, Thermo Scientific) as well as an evaporator (Combidancer, Hettich). Plates are handled by a robotic arm (TX60 L, Stäubli) that allows the transfer between the STARplus module and the various instruments. Sample analysis is performed by mass spectrometry using a Rapid-Fire-Q-TOF combination (Agilent). Results are stored in a proprietary laboratory information system and data evaluation is performed by Excel (Microsoft).

PAMPA

Parallel artificial membrane permeability assay is a primary screen surrogate for gastro-intestinal permeability (passive diffusion). PAMPA assay uses a thin hexadecane layer as a model membrane. The assay is carried out in 96-well plates where the ability of the compound to diffuse from a donor to an acceptor compartment separated by a hexadecane layer coated on a polycarbonate filter plate is measured. To minimize solubility issues compounds are loaded at 5 μM in the donor compartment and the assay buffer contains 5 % DMSO. The permeability is derived from the compound concentration (measured by LC–MS/MS) in the acceptor compartment after a 4-h incubation time (Smith et al. 2014; Di et al. 2012).

Native MDCK

Madin Darby canine kidney (MDCK) cells are an epithelial cell line of canine kidney origin. MDCK cells have low expression of transporter proteins and low metabolic activity. MDCK cells are used as a cellular barrier model to assay polarized transport of compounds of interest through the epithelia. Under standard cell culture conditions, MDCK cells develop tight junctions and form monolayers of polarized cells. The cells are seeded on a 24 well plate (BD Falcon) and form a confluent monolayer within 4 days prior to the experiment. On day 4, the test compound is added to the apical side of the membrane and the transport of the compound across the monolayer is monitored after a 2 h incubation period. For studies related to drug efflux, it is also necessary to examine the transport of the compound from the basolateral compartment to the apical compartment declared as efflux ratio. The permeability in both directions A to B and B to A are derived from the compound concentration (measured by LC–MS/MS) in apical and basal compartments after a 2-h incubation time (Smith et al. 2014; Di et al. 2012).

In Vitro and In Vivo Clearance Experiments

The experiments were performed in 384 PCR plates at 37 °C on an automated Hamilton platform. Test articles (10 mM DMSO solutions) were dispensed by an acoustic dispenser into the PCR plates (5 nL) containing 25 μL of 2 mM NADPH solution (in phosphate buffer pH 7.4). The incubation was started after 10 min pre-incubation by the addition of 12.5 μL compound/NADPH solution to 12.5 μL of a microsomal solution (0.5 mg/mL in phosphate buffer pH 7.4). Reactions were stopped after 0.5, 5, 10 and 30 min by the addition of 10 μL CH_3CN/formic acid (93:7) containing the analytical internal standards (1 μM alprenolol and 1.6 μM chlorzoxazone) and transfer to a new plate containing 15 μL CH_3CN/formic acid (93:7). The samples were then centrifuged at 5,000 *g* at 4 °C for 15 min. Supernatants were pooled by 3 (dilution 1/3) and 10 μL of the pool analyzed by LC–MS(MS) for quantitation of the remaining test articles.

Plasma Protein Binding

Plasma protein binding was evaluated utilizing a rapid equilibrium dialysis (RED) device, a 96-well dialysis method used to measure protein binding of drugs in plasma (mouse CD1 strain). The RED device consists of a Teflon base plate housing disposable dialysis units with a large surface area for rapid equilibrium. The peptide is spiked into plasma and dialysed against Dulbeccos phosphate buffered saline (DPBS) solution at 37 °C under constant agitation.

Aggregation

The assay is based on a Taylor dispersion analysis (TDA), the instrument used is the Viscosizer 200 from Malvern. The samples are injected (plug of 100 mbar during 0.35 min) in a capillary filled with buffer that has two windows for UV detection (wavelength used: 254 nm). The samples are pushed through the capillary by applying a constant pressure (300 mbar). UV data is recorded for the two detection windows. The software then calculates the diffusion coefficient for each sample based on the difference of peak width between the two windows. Hydrodynamic radius (Rh) is then calculated using the Stokes equation (Seidler et al. 2003).

P.O. Study in Mice: Pharmacokinetics of Cyclohexapeptide (1) and Cyclohexapeptide (2)

The pharmacokinetic parameters were estimated using an internal non-compartmental approach, using i.v. and p.o.

administration with and without DDM as an enhancer. Conscious, fed, male OF1 mice (Iffa Crédo, France) were administered a single bolus dose of 3 µmol/kg test substance in NMP:Plasma (10:90), with an i.v. administration volume of 5 mL kg^{-1}. For p.o. application, two different animal groups were dosed by a single bolus dose of 10 µmol/kg test substance in water and 1.5 % dodecylmaltoside (DDM; enhancer, Deshmukh et al. 2010) in water with a p.o. administration volume of 10 mL kg^{-1}. For all mice, sequential blood samples (10 µL, collected by puncture of the lateral saphenous vein) were collected from each animal for up to 24 h after administration and were stored at −20 °C. To determine the concentrations of the test substances, the 10 µL blood samples were used and proteins were precipitated by adding 80 µL of CH_3CN and 20 µL of water containing a generic internal standard. Sample analysis was performed on a LC–MS/MS system consisting of an AB SCIEX API 5500 QTrap mass spectrometer equipped with a TurboIonSprayTM interface (Framingham, USA). The MS system was connected to a HTS CTC PAL auto-sampler (Zwingen, Switzerland) and to a Flux Rheos 2200 pump system (Zwingen, Switzerland). The supernatants (5 µL) were injected directly onto the LC/MS/MS system for analysis. The test article and its internal standard were separated with a Phenomenex POLAR RP (50 × 2 mm ID, 2.5 µm pore size). A binary gradient with a mobile phase consisting of water (A) and CH_3CN (B) was used for the LC-separation. Both mobile phases (A) and (B) were acidified with 1 % formic acid. The elution gradient program was as follows: [(time(min), % mobile phase B): (0, 40) (5, 100) (6, 100) (6.1, 40) (7.5, 40)]. The column temperature was maintained at 50 °C using a column heater. Under these experimental conditions, the lower limit of quantification was 0.4 ng/mL.

X-Ray Structure

Crystalline tri-N-methylated cyclohexapeptide (2) was prepared by dissolving the compound in methanol and letting the solvent evaporate at ambient temperature. Diffraction data were collected with a Bruker AXS SMART 6000 CCD detector on a three-circle platform goniometer with Cu(Ka) radiation (λ = 1.54178 Å) from a Microstar rotating anode generator equipped with Incoatec multilayer mirrors. A semi-empirical absorption correction (SADABS) was applied, based on the intensities of symmetry-related reflections measured at different angular settings (maximum and minimum transmission 0.9684 and 0.4967). The structure was solved by dual-space recycling methods and refined on F^2 with the SHELXTL programs. The tri-N-methylated cyclohexapeptide (2) crystallizes with two independent molecules and one equivalent of water in the orthorhombic space group $P2_12_12_1$. The numbering scheme is shown in Fig. 4. In molecule two, the proline C_γ (CCDC structure C152) and the side chain of Leu^4 (C146–C149) are disordered. The disorder was modeled by refining two different conformations with a 0.59–0.41 distribution for Pro^5 and two different orientations with a 0.63–0.37 distribution for Leu^4. Bond lengths, angles, and displacement parameters of all minor occupancy parts were restrained to be similar to those of the corresponding moieties in molecule 1. For atoms in the major occupancy orientation anisotropic displacement parameters were used, for atoms in the minor occupancy orientation isotropic displacement parameters were used. Hydrogen atoms at carbons were calculated in idealized positions and refined using a riding model with $U_{iso}(H) = 1.2$ or $1.5\ U_{eq}(C)$, hydrogen atoms at hetero atoms were located in difference maps and refined with appropriate geometric restraints.

Superposition of the two crystallographically independent molecules using their C-alpha atoms is possible with an rmsd of 0.358 Å. Significant conformational differences are only observed in the side chains of Pro^5 and Leu^4 (see Fig. 6b and Fig. 2 in the Supplementary Material). In both molecules of tri-N-methylated cyclohexapeptide (2) the conformation of the central ring is stabilized by two intramolecular hydrogen bonds involving the backbone NH and C=O of Leu^1 and Leu^4 (N12–H12···O33 and N3–H3···O50 in molecule 1, N112–H112···O133 and N103–H103···O150 in molecule 2) whereas the hydrogen bonds to the solvent molecules (water) differ: in molecule 1 an additional bidentate hydrogen bond between a water (O55) and the backbone C=O of Leu^2 and Pro^5 (O39 and O54) stabilizes the conformation, in molecule 2 a water (O155) indirectly links two adjacent peptide molecules in the crystal via hydrogen bonds to C=O of Leu^4 in molecule 2 and to the water associated with molecule 1 (O155–H156···O150 and O155–H157···O55).

Final data: $C_{41}\ H_{68}\ N_6\ O_8$; $M_r = 773.01$, crystal size 0.26·0.05·0.05 mm^3 (grown from methanol), orthorhombic, space group $P\ 2_12_12_1$ (No. 19) with $a = 16.763(6)$, $b = 16.896(7)$, $c = 31.500(12)$ Å, $V = 8922(6)$ $Å^3$, $Z = 8$, $D_c = 1.151$ g·cm^{-3}, $\mu = 0.646$ mm^{-1}, $F(000) = 3{,}360$, 183,807 reflections measured, 15,728 independent, $R_{int} = 0.0476$, $2.81° < \theta < 66.59°$, T = 100(2) K, 1,015 parameters, 266 restraints, $R_1 = 0.0335$, $wR_2 = 0.085$ for 14,922 reflections with $I > 2\sigma(I)$, $R_1 = 0.0365$, $wR_2 = 0.0887$ for all 15,728 data, GoF = 1.047, restrained GoF = 1.054, res. el. dens. = + 0.45/−0.21 e $Å^3$.

NMR Experiments

Cyclohexapeptide (1) and tri-N-methylated cyclohexapeptide (2) were prepared from approximately 1 mg in 150 µl DMSO-d_6 and $CDCl_3$-d_1, providing 10 mM solutions of each cyclohexapeptide respectively. All NMR experiments were recorded at 300 K on a Bruker Avance spectrometer with a 1.7 mm TCI Cryoprobe, using a ^1H resonance

frequency of 600.13 MHz and a ^{13}C resonance frequency of 150.90 MHz. Chemical shifts were measured relative to the DMSO-d_6 solvent signal at 2.49 ppm (^{1}H) and 39.6 ppm (^{13}C), and relative to the $CDCl_3$-d_1 solvent signal at 7.26 ppm (^{1}H) and 77.36 ppm (^{13}C), respectively. A series of NMR spectra were measured: 1D-^{1}H, HSQC, COSY, ROESY, and TOCSY. The ROESY spectra were recorded using a standard pulse sequence from Bruker, 32 scans per increment, a data matrix of 400 × 2,048 points, and a mixing time of 200 ms with a spin lock time of 60 µs. The NMR data were processed using the software TOPSPIN 3.1 from Bruker (http://www.bruker.com/products/mr/nmr/nmr-software/software/topspin/overview.html). ROE (Rotating frame Overhauser Effect) data are measured by integration of cross peaks in ROESY spectra. Using the invariant distance between the geminal protons at the Cβ of Tyr-6 as a reference, the distance r_{ij} between a pair of hydrogens i and j is determined from the ROESY peak integral a_{ij} according to

$$r_{ij} = r_{\text{ref}} \left(\frac{a_{\text{ref}}}{a_{ij}} \right)^{\frac{1}{6}}$$

where r_{ref} and a_{ref} are the distance and peak integral of the reference protons, respectively.

Conformational Studies and In-Silico Property Predictions

Both restrained and unrestrained simulations were performed. In the former case, ROE restraints were imposed by a harmonic energy function of the deviation from the experimentally determined distance between hydrogens. ROE distances involving undistinguishable hydrogens were computed by averaging over all atom pairs concerned according to $R_{\text{ave}}^{-6} = \sum R_{ij}^{-6}/N$. The exponent of -6 ensures that the smallest distance dominates and the constraint is fulfilled if the closest hydrogen pair is at the target distance. The harmonic force constant for distances smaller and larger than the experimental ROE distance was set to 1 and 4 kcal/mol/Å^2, respectively. For calculating the time-average ROE distance between hydrogens, we averaged the intensity of the cross-peak over the set of N_{MD} conformations collected during simulation, $R_{\text{MD}}^{-6} = \sum R_k^{-6}/N_{\text{MD}}$. The overall deviation of the hydrogen distances from experiment was computed as the root mean squared deviation, $\text{rmsd}_{\text{ROE}} = \left[\sum \left(R_i^{\text{MD}} - R_i^{\text{ROE}} \right)^2 / N \right]^{1/2}$ where R_i^{MD} and R_i^{ROE} are the simulation distance and the experimental distance of ROE number i, respectively. For a dihedral angle φ involving the backbone atoms C–N–C_α–C, the coupling constant $^{3}J_{HN\alpha}$ was calculated using the Karplus equation (Karplus 1959), and the overall agreement between simulation and experiment was again evaluated as the root mean squared deviation of all coupling constants from the NMR data. The coupling constants were not used as restraints in the simulations, because for some values of $^{3}J_{HN\alpha}$, there are several possible corresponding values of the dihedral angle φ. To obtain a qualitative measure of the conformational flexibility of the peptides, the set of conformations from a simulation was clustered using the root mean squared distance between all heavy atoms (after optimal rotation and translation) and an iterative clustering algorithm first described by van Gunsteren and co-workers was applied (Daura et al. 1999). In this method, the conformation with the largest number of other structures within a given root mean squared distance is defined as the first cluster center; from all structures outside this cluster, the one with the most neighbors is again determined, and the process continued until all conformations are assigned to a cluster. The number of cluster centers can provide information on the flexibility and entropy of a molecule, which is influenced by solvation. To assess the solvent interaction by donors and acceptors, we computed the solvent accessible polar surface area (SAPSA) of the peptides. Consistent with the definition of the polar surface area (PSA) of small molecules, we employed atomic radii as given by Clark (1999). However, different from the definition of the PSA, we computed the surface of a solvent probe sphere with a radius of 1.4 Å in contact with oxygen, nitrogen, and their bonded hydrogens, i.e. the polar part of the solvent accessible surface area that has been widely used in protein structure theory (Connolly 1983; Richmond 1984).

Results

Synthesis

The synthesis of two cyclohexapeptides (1) and (2) first reported by Lokey (Fig. 1, Rezai et al. 2011) is illustrated in Scheme 1. Peptides were synthesized on solid phase using N-α Fmoc protection and to obtain the tri-N-methylated compound (2), two different strategies were considered. On one hand, the global selective N-methylation experiment described earlier, utilizing LiOtBu, was applied to the peptide resin to produce the desired N-methylated cyclic peptide still attached to the solid phase (Scheme 1).

Alternatively, a stepwise assembly using SPPS of the N-methylated linear sequence was carried out followed by cyclisation in solution. As reported by Lokey (Rezai et al. 2011), the first strategy, was most successful as indicated by a highly pure crude product (Fig. 2a) following global N-Methylation in the presence of LitBu. However, if other bases are applied, such as 2 % DBU, the reaction becomes

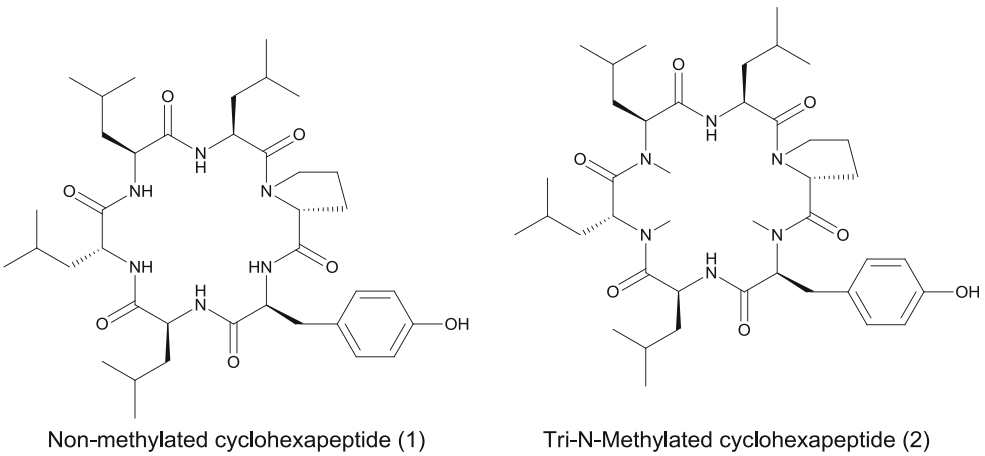

Fig. 1 Non-methylated cyclohexapeptide (*1*) and tri-N-methylated cyclohexapeptide (*2*)

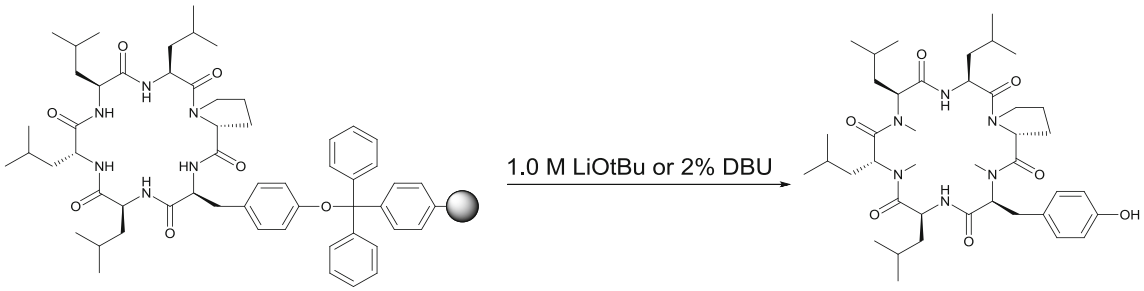

Scheme 1 Global N-methylation of the non-methylated cyclohexapeptide (1) on the solid phase in the presence of the bases indicated

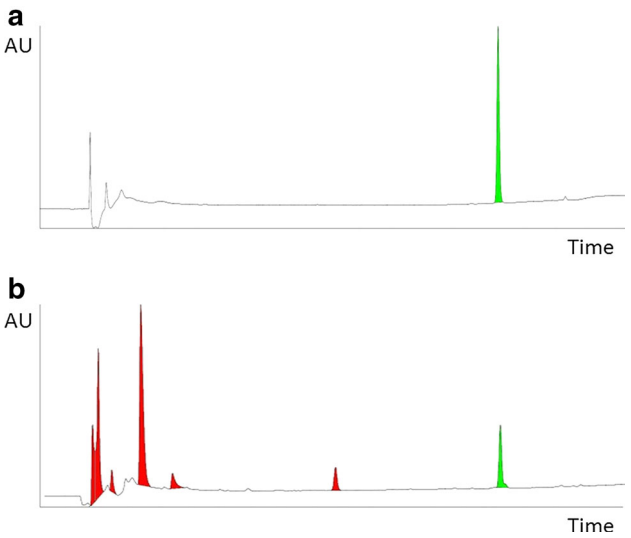

Fig. 2 **a** UPLC after global N-methylation of the solid-phase bound cyclohexapeptide (1) in the presence of 1 M LiOt–Bu in THF. **b** UPLC after global N-methylation of the solid-phase bound cyclohexapeptide (1) in the presence of 2 % DBU in THF

less selective (Fig. 2b). The main product indicated in Fig. 2a was isolated and submitted to NMR analysis to confirm the expected N-methylation pattern as shown in Fig. 1.

Physicochemical Properties and Permeability

Following purification and characterization, both cyclohexapeptides underwent classical profiling. Interestingly, already at the level of solubility, real differences emerge between the non-methylated cyclohexapeptide (1) and the tri-N-Methylated counterpart (2). Cyclohexapeptide (1) is soluble up to 0.15 mM at pH = 6.8, whereas the tri-N-methylated derivative (2) displays a lower solubility of 0.026 mM (Table 1). These experimental results are paralleled by the differences in calculated ClogP and the PSA characteristics (Table 2). Compound (1) exhibits a lower ClogP of 7.5 and a PSA of 186 $Å^2$ compared to ClogP of 9.4, and a PSA of 160 $Å^2$ for the more hydrophobic tri-N-methylated cyclohexapeptide (2). Interestingly, in terms of hydrogen bond donors, the contrast between only 3 H-bond donors present in the cyclohexapeptide (2) and 6 H-bond donors featured in the non-methylated poorly permeable cyclohexapeptide (1) seems to be responsible for the intrinsic difference in properties, while both peptides share the identical number of 13 H-bond acceptors (Table 2). Both peptides were assessed for passive permeability, measured by the PAMPA assay. In addition, permeability was assessed on the cellular level by observing transport through a monolayer of native MDCK-cells. Consistent

Table 1 Solubility and permeability of cyclcohexapeptides

Cyclohexapeptide	Sol/pH 6.8 (mM)	logPe pH 6.8	MDCK/recovery (AB) (%)	MDCK/Papp (AP–BL) [10–6 cm s^{-1}]	Perm. class
(1)	0.15	<−6.5	80	2	L
(2)	0.03	−4.5	75	11	H

Table 2 Calculated properties of cyclcohexapeptides

Cyclohexa peptide	MW	ClogP	PSA [Å^2]	H-bond donors	H-bond acceptors
(1)	712	7.5	186	6	13
(2)	755	9.4	160	3	13

Table 3 In-vitro clearance data of cyclcohexapeptides

Parameter liver microsomes (CYP)	Cyclohexapeptide (1)	Cyclohexapeptide (2)
Hepatic extraction (%)	95	63
$t_{1/2}$ (min)	3.2	36
CL int uL/min mg	433	39

Table 4 Plasma protein binding and aggregation behavior of cyclcohexapeptides

Parameter	Cyclohexapeptide (1)	Cyclohexapeptide (2)
PPB (%)	92.1 ± 0.7	>99 ± 0.7
Aggregation Rh (nm) 20 μM	0.154	0.153
	0.252	0.265
Aggregation Rh (nm) 100 μM		

with the higher polarity for the non-methylated cyclohexapeptide (1) a low permeability at pH = 6.8 of <−6.55 log Pe was measured in the PAMPA assay and this peptide was accordingly classified as a low permeable compound (L). However, under these conditions, for the tri-N-methylated derivative (2) a value of −4.50 was determined in the PAMPA assay, which confirms this molecule to be in the range of a highly permeable compound (H). This difference in permeability properties is supported by results from the native MDCK assay. In this case the non-methylated cyclohexapeptide (1) exhibits a low flow = 2×10^{-6} cm s^{-1} in contrast to the higher flux of 11×10^{-6} cm s^{-1} measured for the tri-N-methylated derivative (2) as illustrated in Table 1.

Oral Uptake Studies in Mice

Since the principal findings of Lokey's previous publications could be confirmed (Rezai et al. 2006, 2011), both peptides were considered for an oral uptake study in mice to determine the absolute oral biovailability. In particular, we were interested to study the effects of the well-known uptake enhancer DDM (Deshmukh et al. 2010). In the next step, in vitro clearance parameters were determined. The differences in solubility and permeability, observed for the two peptides, is also reflected in the in vitro and in vivo clearance (Table 3). C_L is high for the non-methylated cyclohexapeptide (1) (433 μL/min mg). In contrast, the clearance of the tri-N-methylated variant (2) is more than 10 times lower (39 uL/min mg). The in vitro $t_{1/2}$ of the N-methylated derivative is also a factor 10 greater (36 min) compared to 3.2 min for the non-methylated peptide (1). The hepatic extraction of the tri-N-methylated compound (2) at 63 % reflects its greater hydrophobicity compared to 95 % for the non-methylated cyclohexapeptide (1) (Table 3). In addition, plasma protein binding and aggregation properties were studied. Interestingly, a very high plasma protein binding is observed for the tri-N-methylated cyclohexapeptide (2), although the potential for aggregation under these conditions is very similar for both molecules (Table 4). The N-methylated version (2) is >99 % protein bound versus about 92 % in the case of the non-N methylated counterpart (1).

The results of the in vivo p.o. study confirm the contrasting in vitro data and the published values for oral bioavailability (Rezai et al. 2011). Figure 3 provides a time dependence on the average blood levels achieved for the doses indicated. The tri-N-methylated cyclohexapeptide (2) showed a very low clearance (CL) of 1 mL min^{-1} kg^{-1}, a low volume of distribution at steady state (V_{SS}) of 0.4 L/kg and a terminal half live ($t_{1/2}$) of 21.9 h after i.v. administration in mice (Table 5). After p.o. administration without enhancer, the tri-N-methylated cyclohexapeptide (2) exhibits a C_{max}, of 534 nM a moderately late T_{max} of 3.8 h resulting in an oral bioavailability (BAV) of 30 %. The non-methylated cyclohexapeptide (1) showed a very high clearance (CL) of 82 mL min^{-1} kg^{-1}, a low volume of distribution at steady state (V_{SS}) of 0.8 L/kg and a very short half live ($t_{1/2}$) of 0.2 h after i.v. administration in mice. The volume of distribution at steady state (V_{ss}) is not significantly different for both peptides. After p.o. administration without enhancer, the tri-N-methylated cyclohexapeptide (2) exhibits a very low C_{max} of 2.9 nM, an

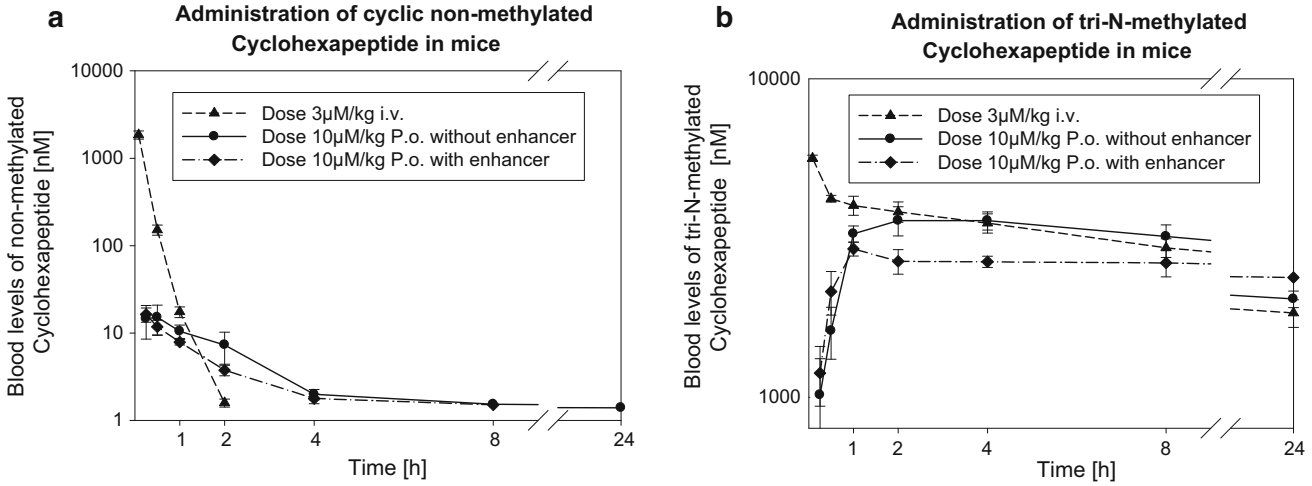

Fig. 3 **a** Blood levels of non-methylated cyclohexapeptide (1) following i.v. and p.o. dosing. **b** Blood levels of tri-N-methylated cyclohexapeptide (2) following i.v. and p.o. dosing

Table 5 In-vivo i.v./p.o. study of cyclohexapeptide (1) and tri-N-methylated cyclohexapeptide (2) ± DDM(1.5 %) as an enhancer in the p.o. part

Parameter	Cyclohexapeptide (1)		Cyclohexapeptide (2)	
Dose [i.v.] (μM/kg)	3		3	
CL (mL min^{-1} kg)	82		1.0*	
V_{ss} (l/kg)	0.8		0.4*	
t1/2term (h)	0.2		21.9*	
AUC i.v. d.n. (nM h)	292		29,618*	
	p.o. without enhancer	p.o. with enhancer	p.o. without enhancer	p.o. with enhancer
Dose [p.o.] (μM/kg)	10	10	10	10
AUC p.o. d.n. (nM h)	5.7	3.6	8,967*	8,046*
BAV (%)	2.0	1.2	30*	27*
Cmax d.n. (nM)	2.9	2.3	534	387
T_{max} (h)	0.6	0.3	3.8	1.0

d.n. dose normalized to 1 mg·kg^{-1}

* Values based on AUC (t-last)

early T_{max} of 0.6 h and a low oral bioavailability (BAV) of only 2 %. Interestingly, DDM applied as an enhancer (Deshmukh et al. 2010) could neither promote oral uptake for the cyclic peptide with high oral BAV, nor for the peptide demonstrating a modest uptake.

As expected from the in vitro profiling, the tri-N-methylated cyclohexapeptide (2) exhibits low in vivo clearance of 1 mL min^{-1} kg^{-1} in contrast to the non-methylated compound (1) which shows 82 mL min^{-1} kg^{-1} (Table 5), demonstrating good agreement with in vitro clearance. The fundamentally different half-life of less than 1 h for the non-N-methylated derivative (1) versus 22 h for the tri-N-methylated peptide (2) is readily explained by the lower clearance (CL), higher area under the curve ($AUC_{i.v.}$), and more prominent protein binding of the tri-N-methylated peptide (>99 %, Table 4). Overall, these studies add some more detail to the previous results (Rezai et al. 2011) obtained in rats, and confirm the hypothesis of the importance for conformational preferences and shielding polar groups, in the light of the beneficial effects for oral uptake if H-bonds can be internalized.

Conformational Studies by NMR and X-Ray

Following up on the PK studies, we used NMR spectroscopy and X-ray to determine the preferred conformations of both cyclic peptides in polar and apolar environments. We were able to obtain crystals from a methanol solution for the tri-N-methylated cyclohexapeptide (2), with the structure being solved at a resolution of 0.84 Å. The corresponding 3D-arrangement indicating two internal H-bonds plus an additional water mediated contact is shown in Fig. 4. Two independent molecules were observed in the unit cell and the only major difference relates to the nature of the H-bond to the water molecule. Since this result from X-ray analysis concurs optimally with the hypothesis of preferred conformations driving permeability by optimizing internalization of H-bonding, we investigated the conformational space in $CDCl_3$ and d^6 DMSO further by application of NMR to cyclohexapeptide (1) and cyclohexapeptide (2).

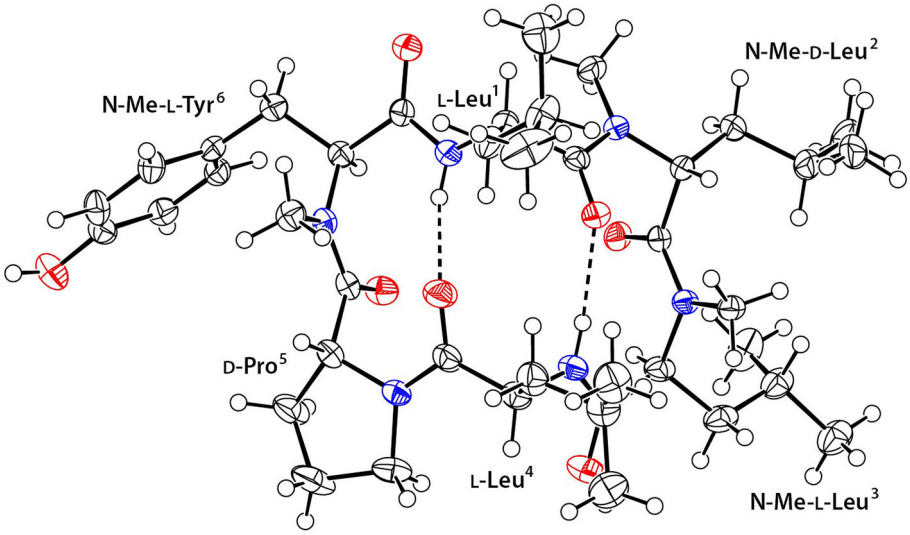

Fig. 4 Structure of tri-N-methylated cyclohexapeptide (2) in the crystal at 0.84 Å resolution (the first out of two independent molecules is displayed). Ellipsoids are shown at the 50 % probability level and radii of hydrogen atoms are arbitrary. Intramolecular hydrogen bonds are marked with *dotted lines*

In principle, we would have liked to compare conformations for both cyclic peptides based on NMR experiments in chloroform and water to match these 3D arrangements against the X-ray structure described above. Our intention was to elucidate, whether there may be preferred conformations responsible for transport across membranes providing further insights. Due to solubility limitations for cyclohexapeptide (2) in water, we decided to apply DMSO as a substitute polar solvent. The ROE distances obtained from the measurements of both peptides in $CDCl_3$ and d^6 DMSO are summarized in Tables 6 and 7. All interproton distances are shorter in $CDCl_3$ than in d^6 DMSO with exception of the ROE peak number 10 of non-methylated cyclohexapeptide (1). This finding may be the result of a more compact structure in $CDCl_3$. Moreover, correlations that would correspond to a pair of consecutive Hα protons at short distance were absent from the ROESY spectra of the cyclohexapeptides, indicating that all amide bonds are in the standard *trans*-configuration in both solvents.

The $J_{HN\alpha}$ coupling constants between the HN and HA protons of each residue are measured from the distance between their peaks in the ^{1}H NMR spectrum and provide information regarding the backbone dihedral angle φ of the corresponding residue. According to the values in Table 8, the coupling constants of residues Leu^3 and Tyr^6 in cyclohexapeptide (1) are significantly lower in $CDCl_3$ than in d^6 DMSO, and lower than the coupling constants of the other residues in either solvent. Assuming the peptide adopts the conformation of a minimal, cyclic hairpin, the coupling constants of the non-methylated cyclohexapeptide (1) in $CDCl_3$ indicate the involvement of residues 3 and 6 in the turns. In the more polar DMSO, no preferred turn position as measured by the coupling constants is observed.

Table 6 ROE cross peaks and derived distance constraints for the non-methylated cyclohexapeptide (1)

Integral	Solvent		d^6 DMSO	$CDCl_3$
	Peak-1	Peak-2	Distance (Å)	Distance (Å)
1	6-HB1	6-HB2	1.75	1.75
2	1-HN	2-HN	3.12	2.29
3	1-HN	4-HN	3.92	3.76
4	1-HN	6-HN	2.61	2.56
5	3-HN	4-HN	2.49	2.30
6	4-HN	1-HN	–	3.60
7	4-HN	2-HN	4.36	3.07
8	4-HN	3-HN	2.42	–
9	1-HN	1-HA	2.97	2.54
10	1-HN	5-HA	3.22	3.60
11	1-HN	6-HA	3.22	2.95
12	4-HN	2-HA	4.47	4.20
13	4-HN	3-HA	3.43	3.19
14	4-HN	4-HA	2.95	2.65
15	6-HD	6-HN	3.04	2.69
16	6-HD	1-HA	–	3.50
17	6-HD	6-HA	2.86	2.47

For tri-N-methylated cyclohexapeptide (2), only the coupling constants of residues Leu^1 and Leu^4 can be measured, and are consistent with an extended-β conformation. Furthermore, these results imply that irrespective of the solvent, the extended conformation of Leu^1 and Leu^4 is more dominant for tri-N-methylated peptide (2) than for non-methylated peptide (1).

These experimental NMR data were used to calculate preferred conformations for both cyclic hexapeptides in $CDCl_3$ and d^6 DMSO.

Table 7 ROE cross peaks and derived distance constraints for tri-N-methylated cyclohexapeptide (2)

Integral	Solvent		d^6 DMSO	$CDCl_3$
	Peak-1	Peak-2	Distance (Å)	Distance (Å)
1	6-HB1	6-HB2	1.75	1.75
2	1-HN	2-HNMe	4.28	4.04
3	1-HN	4-HN	3.47	3.10
4	1-HN	6-HNMe	2.81	2.54
5	4-HN	1-HN	4.06	3.50
6	4-HN	3-HNMe	2.66	2.44
7	1-HN	1-HA	3.06	2.78
8	1-HN	5-HA	3.94	3.59
9	1-HN	6-HA	2.85	2.58
10	4-HN	2-HA	3.77	3.33
11	4-HN	3-HA	2.97	2.70
12	4-HN	4-HA	2.99	2.72
13	6-HD	6-HNMe	3.19	2.86
14	6-HD	1-HA	–	–
15	6-HD	6-HA	2.64	2.28

Table 8 $J_{HN\alpha}$ coupling constants observed in d^6 DMSO and $CDCl_3$

Solvent	Cyclohexapeptide (1)		Cyclohexapeptide (2)	
	d^6 DMSO	$CDCl_3$	d^6 DMSO	$CDCl_3$
Leu1	8.1	8.8	9.4	9.4
Leu2	7.1	8.1	–	–
Leu3	8.1	5.9	–	–
Leu4	8.1	8.8	8.9	8.9
Tyr6	8.6	5.9	–	–

Simulations and In Silico Property Predictions

Aiming at a more comprehensive understanding of the conformational preferences and physico-chemical properties of the cyclohexapeptides (1) and (2) at the atomic level, extensive molecular dynamics simulations were performed. In this case, the CHARMm program (Brooks et al. 1983) was applied and analysis was pursued using tools developed in-house. We compared the set of structures generated by unconstrained simulation with ROE distances and J-coupling constants from NMR experiments, and molecular dynamics simulations with ROE restraints were performed to identify the solution structure of the peptides in DMSO and chloroform. Furthermore, for the assessment of conformational flexibility, we clustered the structures generated by the simulations according to the root mean squared distances (rmsd) between conformations and calculated the solvent-exposed polar surface area.

We performed unconstrained and constrained molecular dynamics simulations of the cyclohexapeptides in implicit solvent models (Schaefer and Karplus 1996; Schaefer et al. 1998) of water and chloroform as described in the "Materials and Methods" section. The rmsd of the computed hydrogen distances from the ROE distances in Tables 6 and 7 are represented in Fig. 5a and c for the non-methylated cyclohexapeptide (1), and Fig. 5b and d for tri-N-methylated cyclohexapeptide (2), respectively. Excluding the first ns of the simulations, which may be biased by the starting conformation, the rmsd varies from 0.3 to 1.9 Å for non-methylated cyclohexapeptide (1), and between 0.1 and 2.0 Å for tri-N-methylated cyclohexapeptide (2) in DMSO. For the simulations in chloroform, the range of the ROE rmsd is 0.2–1.2 Å for (1) and from 0.2 to 1.5 Å for (2), respectively. We determined simulation-average hydrogen distances from the trajectories by averaging over intensities. The rmsd of the time-average ROE distances from experiment are provided in Table 9 for both the unconstrained and the constrained simulations, together with the minimum rmsd deviation encountered during simulation. The structures corresponding to the minimum rmsd deviation can be viewed as the conformations that overall best fit the ROE data. There are only small differences due to use of the ROE constraints, in particular with respect to the minimum rmsd. This is consistent with the observed small deviation of the calculated average hydrogen distances from the experiments in the range from 0.19 to 0.46 Å, which corresponds to constraint forces of up to 0.4 kcal/mol/$Å^2$. These values are small in comparison with thermal noise. Moreover, we compared the conformations with the smallest rmsd between calculated and experimental ROEs from the constrained and unconstrained simulations and found only minor structural differences with the rmsd in the range from 0.25 to 0.40 Å for the backbone heavy atom positions. As a result for the cyclohexapeptides (1) and (2) investigated in this study, it is possible to explore conformational space and identify structures in close agreement with the experiments during 20 ns of unconstrained molecular dynamics simulation. Therefore, the following considerations will be based only on the unconstrained molecular dynamics calculations. We also compared the coupling constants of the backbone N and C_α protons between simulation and experiment and found rmsd differences varying in a wide range from 0.24 to 4.6 for non-methylated cyclohexapeptide (1), and 0.01–5.9 for tri-N-methylated cyclohexapeptide (2), irrespective of the solvent. For the structures with the lowest ROE rmsd in chloroform, the rms deviation of the coupling constants from the NMR data was 1.8 for the non-methylated cyclohexapeptide (1), and 0.5 for the tri-N-methylated cyclohexapeptide (2) (only two measurable coupling

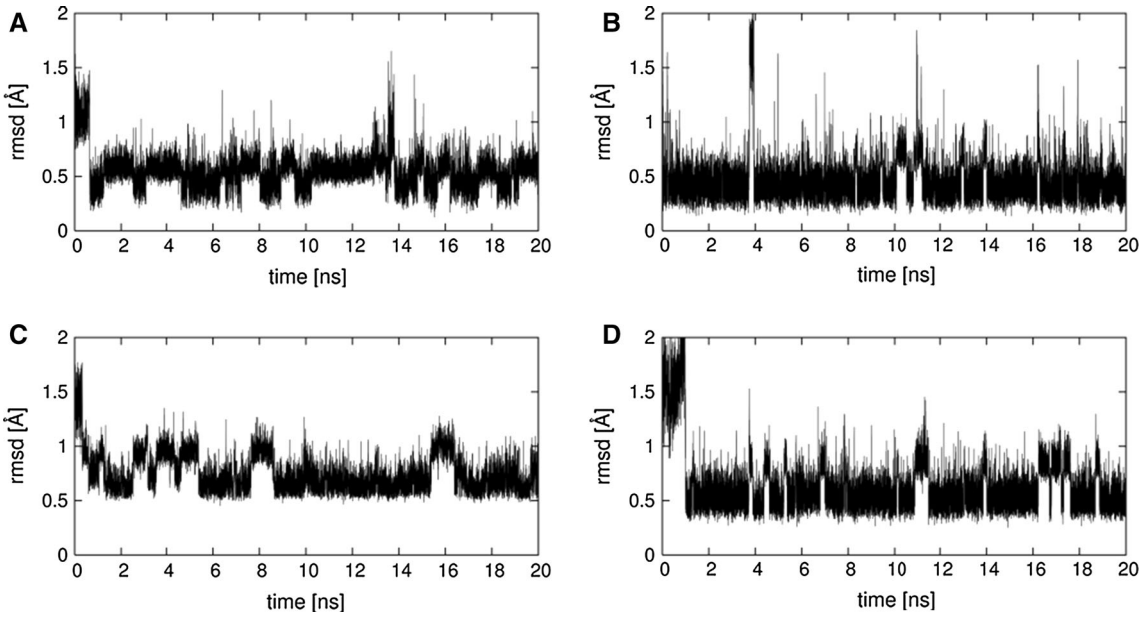

Fig. 5 rmsd of the hydrogen distances from ROE distances during MD simulation of non-methylated cyclohexapeptide (1) in DMSO (*panel A*) and $CDCl_3$ (*panel C*), and tri-N-methylated cyclohexapeptide (2) in DMSO (*panel B*) and $CDCl_3$ (*panel D*)

Table 9 rmsd of simulation-average ROE distances and minimum rmsd from experiment for unconstrained and constrained MD simulation

	Peptide	Unconstrained		Constrained	
		DMSO (Å)	$CDCl_3$ (Å)	DMSO (Å)	$CDCl_3$ (Å)
rmsd of average ROEs	(1)	0.39	0.41	0.29	0.46
	(2)	0.26	0.34	0.19	0.26
Minimum ROE deviation	(1)	0.12	0.45	0.10	0.40
	(2)	0.12	0.25	0.09	0.21

constants). The somewhat larger discrepancy between simulation and experiment for non-methylated cyclohexapeptide (1) may be a consequence of the higher flexibility of this peptide in comparison with tri-N-methylated cyclohexapeptide (2), such that the NMR data cannot be explained by a single conformation but requires consideration of a conformation ensemble.

Figure 6a illustrates the minimum ROE-rmsd solution NMR structure of non-methylated cyclohexapeptide (1) (Schaefer et al. 1998). In fact, the "best" (minimum ROE rmsd) $CDCl_3$ solution structure of non-methylated cyclohexapeptide (1) bears some similarity with tri-N-methylated cyclohexapeptide (2) in the Pro-Tyr turn region. In particular, the H-bond from NH of Leu^1 to C = O of Leu^4 represents a common structural feature. However, the beta-bridge pattern is broken, which would involve the H-bond NH(Leu^4)…C=O(Leu^1) as in Fig. 6b. Instead, cyclohexapeptide (1) forms two different H-bonds in the structure shown, one involving NH(Leu^2)…C=O(Pro^5), and another, weak H-bond with NH(Leu^3)…C=O(Leu^2). The Tri-N-methylated cyclohexapeptide (2) cannot form these H-bonds, since the amide nitrogens of Leu^2 and Leu^3 are methylated. Overall, the best ROE "chloroform solution" structure of non-methylated cyclohexapeptide (1) shows that the non-methylated peptide tries to maximize the number of internal H-bonds. It, therefore, departs from the type II′-beta-bridge pattern of tri-N-methylated cyclohexapeptide (2), which enables only 2 internal H-bonds.

Figure 6b shows a superposition of the NMR solution structure of the tri-N-Methylated cyclohexapeptide (2) (minimum ROE rmsd) in chloroform with its crystallographic structure. There is excellent agreement with respect to the backbone conformation (backbone rmsd 0.23 and 0.36 Å with respect to crystal form 1 and 2, respectively). The side chain orientation is similar between the NMR solution structure and at least one of the crystal forms for all residues with the exception of Leu^3. The differences in the side chain orientations can be explained by the absence of crystal contacts in the simulations. Moreover, energy differences between conformations with the same backbone structure but different side chain dihedral angles can be expected to be small in solution. The main structural features of the peptide structure in the apolar environment and the crystal are a central β-bridge with backbone hydrogen bonds between Leu^1 and Leu^4, flanked by type II' turns formed by (D)-Leu^2-Leu^3 on one side and by (D)-Pro^5-Tyr^6 on the other side (Kabsch and Sander 1983; Hutchinson and Thornton

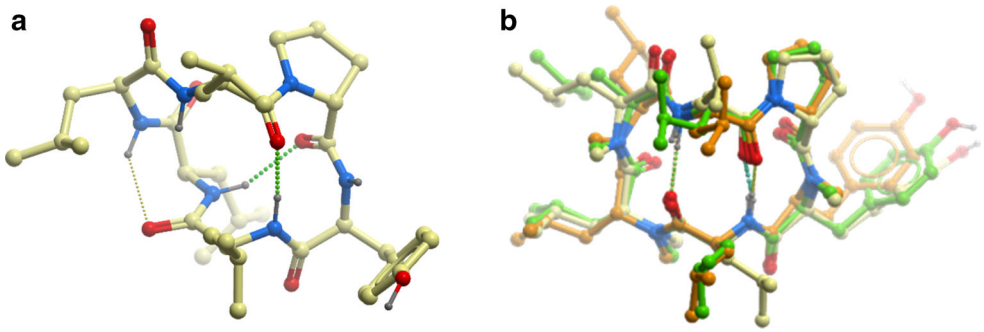

Fig. 6 **a** Minimum ROE-rmsd solution NMR structure in $CHCl_3$ of cyclohexapeptide (1). **b** Superposition of minimum ROE-rmsd solution NMR structure in $CHCl_3$ (*orange carbons*) with structures of cyclohexapeptide (2) from X-ray analysis (crystal molecule 1: *green*; crystal molecule 2: *yellow carbons*)

Table 10 Backbone dihedral angles of the crystallographic structure of cyclohexapeptide (2)

Residue	Crystal form 1			Crystal form 2		
	ω	φ	ψ	ω	φ	ψ
Leu1	−173.1	−127.3	89.1	−174.3	−128.3	91.2
Leu2	−178.4	66.9	−127.5	174.4	76.9	−125.1
Leu3	177.3	−102.3	16.0	−179.4	−103.1	20.8
Leu4	177.1	−108.3	105.7	179.9	−139.5	129.9
Pro5	179.8	55.2	−122.2	178.4	55.3	−137.6
Tyr6	179.6	−103.3	27.2	176.8	−99.2	26.4

1994; Calimet et al. 2001). The characterization of the residues in terms of secondary structure follows from the backbone dihedral angles (see Table 10), which belong to the β-strand region of the Ramachandran plot for Leu^1 and Leu^4, and from the high coupling constants of Leu^1 and Leu^4 for tri-N-methylated cyclohexapeptide (2) in chloroform (Table 8). These findings are also consistent with the use of D-amino acids in the first position of each β-turn, since the dihedral angles are in the ε-region of the Ramachandran plot, corresponding to the energetically favorable β-basin of L-amino acids (Ramachandran et al. 1963). In summary, the solution structure of tri-N-methylated cyclohexapeptide (2) as well as its crystal structure can be characterized by the secondary structure notation BTTBTT, where B indicates a β-bridge formed by Leu^1 and Leu^4, and the TT combination indicates a type II' turn.

For analyses of the dynamics and the influence of the solvent environment, we clustered the conformations generated by molecular dynamics simulation according to their heavy atom rmsd deviation with a cut-off distance of 1.5 Å. Members of the cluster for the two cyclohexapeptides apparent during simulations in chloroform and DMSO are shown in Fig. 7. Clusters are numbered consecutively according to their importance. From the continuous distribution of clusters, most conformations are visited numerous times during 20 ns, indicating that the simulation and conformer distribution has reached equilibrium. As a measure of conformational freedom, we computed the number of clusters for the peptides, and the ratio of the numbers for chloroform and DMSO (Table 11). This ratio can be used as a simple measure of the conformational entropy contribution to the free energy change on transfer from DMSO to chloroform according to $-T\Delta S = -RT\ln(n_{CHCl_3}/n_{DMSO})$. For non-tri-methylated cyclohexapeptide (1) and tri-N-methylated cyclohexapeptide (2), we calculated entropy changes of 0.4 and 0.0 kcal/mol (clustering radius of 1.0 Å), i.e. the non-methylated cyclohexapeptide experiences a loss of entropy on transfer to the low polar medium. By contrast, there is no loss of conformational freedom for the tri-N-methylated cyclohexapeptide (2). Whereas the number of clusters depends strongly on the cluster radius used, the estimate of the entropy change is fairly independent of the rmsd cutoff. For the cluster radius in the range from 1.0 to 1.5 Å, the calculated entropy contribution varies in a narrow range <0.1 kcal/mol. The deviations for smaller clustering radii are due to the fact that there are an increasing number of clusters with only a single conformation, leading to poor statistics for radii <1 Å. The number of clusters is significantly lower for tri-N-methylated cyclohexapeptide (2) than for non-methylated cyclohexapeptide (1) in both solvents, and in fact, the dynamics of the tri-N-methylated cyclohexapeptide is compromised by sterical hindrance. Even the increased strength of internal hydrogen bonds in the apolar chloroform does not lead to a significant change with respect to the conformer distribution.

For a more quantitative analysis of differences between the solvent interactions of non-methylated cyclohexapeptide (1) and tri-N-methylated cyclohexapeptide (2), we computed the 3-dimensional solvent-accessible polar surface area (SAPSA) of the solution structures in chloroform, which can be considered as representative for the conformations adopted during membrane transition. The SAPSA differs from the polar surface area (PSA), which is widely used to estimate the bio-availability of small molecules, since the area is computed for a solvent probe sphere in contact with nitrogen, oxygen, and their bound hydrogen atoms, rather than the surface on the atoms themselves. As a consequence, the SAPSA takes the solvent-accessibility

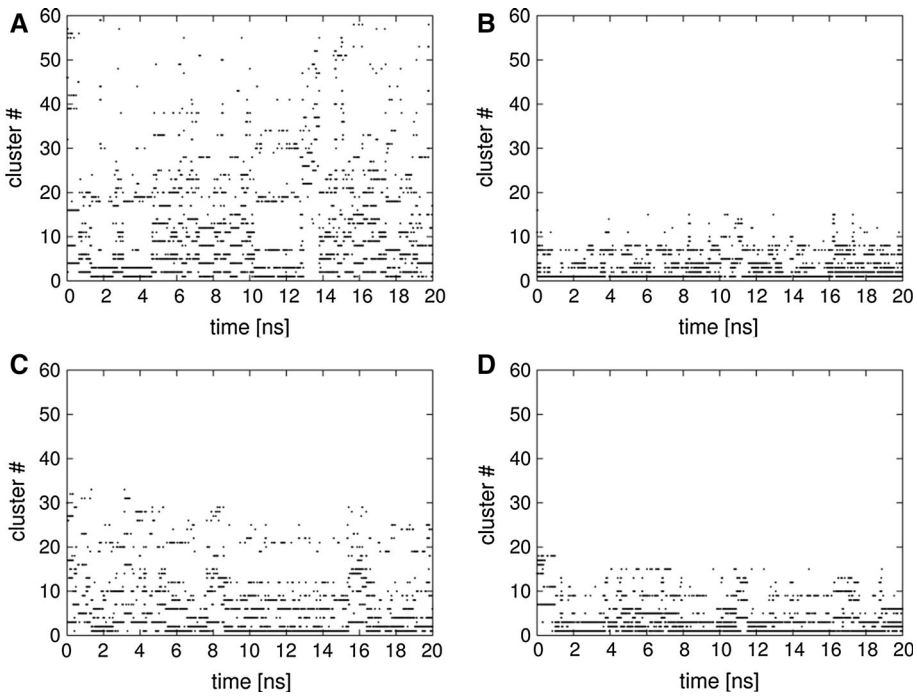

Fig. 7 Occupation of structural clusters during MD simulation of non-methylated cyclohexapeptide (1) in DMSO (*panel A*) and $CDCl_3$ (*panel C*), and tri-N-methylated cyclohexapeptide (2) in DMSO (*panel B*) and $CDCl_3$ (*panel D*)

Table 11 Number of cluster centers and conformational entropy difference on transfer from DMSO to $CDCl_3$ (see text) as a function of clustering radius used

Radius (Å)	Cyclohexapeptide (1)			Cyclohexapeptide (2)		
	N_$CDCl_3$	N_DMSO	$-T\Delta S$ [kcal/mol]	N_$CDCl_3$	N_DMSO	$-T\Delta S$ (kcal/mol)
0.8	910	1,455	0.280	547	582	0.037
0.9	551	949	0.324	284	279	−0.011
1.0	290	594	0.427	167	162	−0.018
1.1	183	363	0.408	100	95	−0.031
1.2	108	200	0.367	65	59	−0.058
1.5	33	59	0.346	18	16	−0.070

of polar atoms into account and the ability of a solute to form intra-molecular hydrogen bonds that are "masked" from the solvent. Table 12 shows the SAPSA of the cyclohexapeptides (1) and (2) for the chloroform NMR solution structure, the average, and the range during DMSO and chloroform simulations. For comparison, the SAPSA is also calculated for a hypothetical "extended" conformation (i.e., ignoring the cyclic closure), in which the polar atoms are fully solvent-exposed. As indicated in Table 12, the SAPSA of the peptides is significantly reduced in their non-polar solvent configurations. However, there is an additional reduction in the polar surface area of tri-N-methylated cyclohexapeptide (2) relative to that of non-methylated cyclohexapeptide (1) due to the methylation of the 3 backbone NH positions. Moreover, the peptides with their molecular weight of 713 and 755 Da, respectively, can be considered as small molecules. As a consequence, methylation of 3 donors in tri-N-methylated cyclohexapeptide (2) is essential to reduce the solvent accessible polar surface area from a borderline case to a value well within the limits for which good passive

Table 12 Solvent accessible polar surface area of cyclohexapeptides (1) and (2)

	Cyclohexapeptide (1) (Å^2)	Cyclohexapeptide (2) (Å^2)
TPSA	186.0	159.7
SAPSA Extended	170.6	150.8
SAPSA $CDCl_3$ solution structure	124.5	108.4
SAPSA DMSO average (σ)	137 (15)	121 (10)
SAPSA $CDCl_3$ average (σ)	126 (12)	119 (10)
SAPSA DMSO range	78–202	84–162
SAPSA $CDCl_3$ range	79–180	76–160

membrane permeability of small molecules can be observed.

Discussion

Repetition of the global methylation experiment reported earlier (Rezai et al. 2011) clearly indicated the sensitivity of this approach regarding the conditions, e.g. the base to produce the optimal N-methylation pattern relevant for membrane passage. According to these results, it seems every scaffold has to be investigated separately to verify, whether a unique species becomes apparent using an optimized protocol. Thus, it seems unlikely that a synthetic methodology could answer the question what would be an optimal N-methylation strategy for a given cyclic peptide. Nevertheless, the classical permeability assays worked reliably for these two cyclic peptides and were absolutely in line with results from in vivo experiments. Especially for larger peptides, physico-chemical properties, in particular the tendency for aggregation, and the effort for proper bioanalysis required for cellular and in vitro-assays are thought to represent the major obstacles to achieve an unambiguous read-out. However, for the two peptides investigated, although solubility in water was quite low for the tri-N-methylated version, no difficulties in this respect were encountered. In addition, the aggregation properties of the non-methylated cyclohexapeptide (1) and the tri-N-methylated cyclohexapeptide (2) are quite similar, and thus, results are really comparable from this perspective. In our view, the combination of very high plasma protein binding and the lower clearance in the liver both contribute importantly to the longer $t_{1/2}$ of the tri-N-methylated cyclohexapeptide (2). In fact, the in vitro clearance data utilizing liver microsomes accurately predicts the in vivo behavior for both cyclohexapeptides. Most significantly for the design of orally available peptidic macrocycles, high plasma protein binding, high permeability and the lower clearance in the liver result in the advantageous BAV of 30 % for the tri-N-methylated cyclohexapeptide. A macrocycle, which has made its way to clinical trials, TZP-101 or ulimorelin, shares some properties with cyclohexapeptide (2). Similarly, a 24 % oral bioavailability was determined in both rats and monkeys for this cyclic molecule (Hoveyda et al. 2011).

The important role of plasma protein binding in influencing the efficacy of a drug has been recently discussed by Liu (Liu et al. 2014). For this reason, hydrophilic modifications promoting permeability would be of interest to adjust plasma protein binding and to enable further development on the basis of a soluble monomeric peptide. A study on unusual nitrogen-containing amino acids, designed to enable H-bonds to the backbone, provides evidence for shielding of the backbone according to in silico and experimental data (Rafi et al. 2012). This kind of modification can be applied to fine-tune properties, e.g. half-life due to optimized protein binding, while maintaining permeability properties. Interestingly, our observations concerning higher hydropobicity and lower clearance resulting in longer half-life are reflected in the comparison of the two marketed drugs octreotide and pasireotide. The PK profile of pasireotide is characterized by fast absorption, low clearance, long half-life, and extensive distribution in healthy volunteers. Compared with octreotide, which has a mean $t_{½}$ of approximately 1.7 h (Ma et al. 2005), pasireotide has a much longer half-life, which is not surprising considering that its chemical structure is more metabolically stable than that of octreotide (Golor et al. 2012). In general, exposure of hydrophobic surface area is more likely to promote permeability and may offer benefits beyond uptake, e.g. for chronic diseases (Rand et al. 2012). Interestingly, the enhancer DDM neither had a positive effect on the oral bioavailability of the highly permeable tri-N-methylated cyclohexapeptide (2), nor on uptake of the less permeable non-methylated counterpart. However, further investigations would be required to clarify, whether enhancers may promote uptake for this particular type of peptides.

Structural investigations and simulations of cyclohexapeptides (1) and (2) show a higher level of mobility for the non-methylated cyclohexapeptide (1) as compared to the tri-N-methylated cyclohexapeptide (2) in both chloroform and DMSO. The highly permeable cyclic peptide (2) thus behaves differently from the well-known CsA, which has been described as a chameleon-type of molecule due to its conformational flexibility (El Tayar et al. 1993; Alex et al. 2011). By contrast, in the case of cyclohexapeptide (2), the conformation is locked as indicated by NMR measurements in both the polar and the apolar environment. As a conclusion from this study, flexibility is not really mandatory to achieve permeability, however, the rigidity of a given scaffold can provide an obstacle for drug development, since target recognition may be compromised. Overall, the results of the simulations confirm the findings from solution structure work and are consistent with the hypothesis that stabilization of internal hydrogen bonding and the reduction of the polar solvent-accessible surface area increase the passive membrane permeability (Rezai et al. 2006). At least in this case, we have demonstrated the potential of theoretical calculations for prediction of a 3D-PSA to support molecular design in favor of high permeability. Therefore, we believe this methodology, applied to preferred conformations obtained from molecular dynamics, represents a useful in silico strategy for property prediction. Of course verification on additional scaffolds different in size and shape is required to prove the

generality, nevertheless, the application to conformationally restricted macrocycles seems straight forward.

In the context of macrocyclic drugs, a more comprehensive analysis of the properties as well as the impact of intramolecular hydrogen bonding leading to favorable properties has recently been outlined (Giordanetto and Kihlberg 2014; Over et al. 2014). In the first of these analyses, Giordanetto and Kilhlberg discuss, what medicinal chemists can learn from the subset of 34 orally administered macrocycles out of a total group of 100 macrocyclic drugs and clinical candidates. Cyclization, compact β-turns, and increased lipophilicity, particularly as MW moves from 700 to 1,000 Da, as well as a PSA between 180 and 240 $Å^2$ were features recognized as contributing favorably towards permeability and oral bioavailability (Knipp et al. 1997; Okumu et al. 1997; Rezai et al. 2006). In the second study, the role of stereoisomerism in enabling optimal formation of an intramolecular H-bond lowering solubility, while increasing lipophilicity was recognized as being pivotal in enabling high cellular permeability. However, new types of analyses and assay formats are required to deepen our understanding of permeability. The correlation of independent data sets on polarity and permeability is a prerequisite to verify for which size and molecular category, certain permeability profiling methodologies may be applied. Recently, a simple alternative to determine polar surface area, advantageous in terms of throughput and material consumption, has been proposed (Goetz et al. 2014a, b). This high throughput SFC method is able to discriminate molecules forming intramolecular hydrogen bonds and isomers lacking this ability. The approach has been extended to cyclic peptides including CsA, and accordingly, peptides enabling internalization of H-bonds exhibit lower retention than similar compounds, that cannot form intramolecular hydrogen bonds. Interestingly, the chromatographic results were confirmed by NMR chemical shift and temperature coefficient experiments. In view of this study, further correlation of innovative variants other than N-methylation and new permeability assays should be investigated to confirm validity of the assay panel on an even broader basis. In fact, modifications cited earlier (Rafi et al. 2012) suggest an alternative to N-methylation, utilizing nitrogen substituted amino acids as an approach to mask polar groups by enabling side chain to side chain or side chain to backbone interactions. This idea may help to arrive at more hydrophilic macrocycles still able to permeate membranes. So far, investigations on polar side chains introduced to cyclohexapeptide (2) have exemplified a drastic loss in permeability for most of these derivatives (Rand et al. 2012). Thus, the introduction of functionality for this type of peptides represents a challenge with respect to maintaining or even improving permeability. Alternative modifications on the backbone promoting permeability are known from natural products such as Sanguinamide (Nielsen et al. 2012). In this case, a thiazole applied as heterocyclic amide isoster was developed by nature, and is thought to inspire future design of macrocycles. Other types of interactions, such as π-cation pairs, may assist in shielding polar groups and reducing PSA, while stabilizing a given scaffold at the same time. These hypotheses, aimed at reducing PSA either by replacing amide bonds with isosters, optimizing H-bond shielding across the macrocyclic ring system, or by optimizing side-chain to backbone interaction have to be investigated across various cyclic peptides of different sizes and conformations. More systematic experiments will help to understand scope and limitations of these various modifications with respect to permeability for a given cyclic structure and enable more reliable predictions for new scaffolds. In summary, pursuing a strategy of masking polar hydrogen bonding groups by internal pairing across the macrocyclic ring is important to improve on permeability, and N-methylation of exposed amides is regarded as only one tool in the box to optimize the properties of cyclic peptides.

Conclusions

We and others have shown the potential of N-methylation to conformationally constrain peptides and obtain highly permeable molecules. Stabilized and modified in the right fashion, they can cross membranes and are even able to achieve significant oral uptake. Without doubt, the understanding of these properties governing permeability and oral bioavailability of macrocyclic peptides is an important and rapidly emerging topic. In this study, we have confirmed ideas communicated earlier and generated a more detailed understanding regarding the factors influencing uptake of cyclic hexapeptides. Interestingly, the intrinsic properties of these cyclic peptides seem to be influential on their oral bioavailability, whereas the role of enhancers to promote oral uptake still has to be explored in more detail. While this manuscript was in preparation, derivatives of this scaffold have been communicated opening up opportunities to achieve oral uptake in the absence of N-methylation (Hill et al. 2014). Nevertheless, shielding of polar surface is mandatory, and in this case, large hydrophobic residues have been shown to help in this respect. For drug development, the balance of overall hydrophobicity and the incorporation of hydrophilic groups is important to keep solubility at a level to enable optimisation. Thus, there is a need to identify modifications enabling transport across the membrane, while keeping the peptide in a soluble state, and preferably in the monomeric form.

A deeper understanding of transport processes and a more profound knowledge of generic modifications

improving permeability is desperately needed to streamline the discovery process for therapeutic peptides. Looking ahead, the design and combination of the structural features enhancing permeability and ultimately oral bioavailability, may be transposed into the design of novel macrocyclic peptides. Ultimately, a collection of various scaffolds intrinsically able to pass through membranes will have a considerable impact on drug development for challenging targets like intracellular protein–protein interactions. In fact, further studies are being actively considered to shed more light on the limits and governing rules for permeable peptides with respect to size, shape, and polarity. Hopefully these type of investigations will enable a path forward to further identify preferred scaffolds and important modifications on side-chains and the backbone to enhance our understanding how to make peptides more amenable for passage through membranes. Steps in this direction are considered to have a large impact on novel therapeutic macrocyclic peptides, since peptidic macromolecules, either orally active or able to address intracellular targets, will lead to a major expansion of the therapeutic peptide market.

Supporting Information

Crystallographic data (excluding structure factors) have been deposited with the Cambridge Crystallographic Data Centre as supplementary publication number CCDC 1039724. Copies of the data can be obtained free of charge on application to CCDC, 12 Union Road, Cambridge CB2 1EZ, UK [fax (+44) 1223 336033, email: deposit@ccdc.cam.ac.uk].

Acknowledgments The excellent support of Sandrine Desrayaud, Valerie Cordier, Elisabeth Braun, Laurent Hoffmann and Francis Risser is gratefully acknowledged. We thank Armin Widmer (armin.widmer@novartis.com) for the molecular modeling program Witnotp.

Conflict of interest Ian Lewis, Michael Schaefer, Trixie Wagner, Lukas Oberer, Emine Sager, Peter Wipfli and Thomas Vorherr declare that they have no conflict of interest concerning Human and Animal Rights and Informed Consent.

References

Alex A, Millan DS, Perez M, Wakenhut F, Whitlock GA (2011) Intramolecular hydrogen bonding to improve membrane permeability and absorption in beyond rule of five chemical space. Med Chem Commun 2:669–674

Bockus AT, McEwen CM, Lokey RS (2013) Form and function in cyclic peptide natural products: a pharmacokinetic perspective. Curr Top Med Chem 13:821–836

Brooks BR, Bruccoleri RE, Olafson BD, States DJ, Swaminathan S, Karplus M (1983) CHARMM: a program for macromolecular energy, minimization, and dynamics calculations. J Comput Chem 4:87–217

Calimet N, Schaefer M, Simonson T (2001) Protein molecular dynamics with the generalized born/ACESolvent model. Proteins: structure. Funct Genet 45:144–158

Chan WC, White PD (2000) Fmoc solid phase peptide synthesis, the practical approach series. In: Hames BD (ed), Oxford University Press, Oxford

Chatterjee J, Gilon C, Hoffman A, Kessler H (2008) N-methylation of peptides: a new perspective in medicinal chemistry. Acc Chem Res 41(10):1331–1342

Clark DE (1999) Rapid calculation of polar molecular surface area and its application to the prediction of transport phenomena, 1. Prediction of intestinal absorption. J Pharm Sci 88(8):807–814

Connolly ML (1983) Solvent-accessible surfaces of proteins and nucleic acids. Science 221(4612):709–713

Daura X, Gademann K, Jaun B, Seebach D, van Gunsteren WF, Mark AE (1999) Peptide folding: when simulation meets experiment. Angew Chem Int Ed 38:236–240

Deshmukh DD, Nagilla R, Ravis WR, Betageri GV (2010) Effect of dodecylmaltoside (DDM) on uptake of BCS III compounds, tiludronate and cromolyn, in Caco-2 cells and rat intestine model. Drug Deliv 17(3):145–151

Di L, Artursson P, Avdeef A, Ecker GF, Faller B, Fischer H, Houston JB, Kansy M, Kerns EH, Kramer SD, Lennernäs H, Kiyohiko S (2012) Evidence-based approach to assess passive diffusion and carrier-mediated drug transport. Drug Discov Today 17(15–16):905–912

El Tayar N, Mark AE, Vallat P, Brunne RM, Testa B, van Gunsteren WF (1993) Solvent-dependent conformation and hydrogen bonding capacity of cyclosporin A: evidence from partition coefficients and molecular dynamics simulations. J Med Chem 36:3757–3764

Giordanetto F, Kihlberg J (2014) Macrocyclic drugs and clinical candidates: what can medicinal chemists learn from their properties? J Med Chem 57:278–295

Goetz GH, Farrell W, Shalaeva M, Sciabola S, Anderson D, Yan J, Philippe L, Shapiro MJ (2014a) High throughput method for the indirect detection of intramolecular hydrogen bonding. J Med Chem 57(7):2920–2929

Goetz GH, Philippe L, Shapiro MJ (2014b) EPSA: A novel supercritical fluid chromatography technique enabling the design of permeable cyclic peptides. ACS Med Chem Lett. doi: 10.1021/ml500239m

Golor G, Hu K, Ruffin M, Buchelt A, Bouillaud E, Wang Y, Maldonado M (2012) A first-in-man study to evaluate the safety, tolerability, and pharmacokinetics of pasireotide (SOM230), a multireceptor-targeted somatostatin analog, in healthy volunteers. Drug Des, Dev Therapy 6:71–79

Hill TA, Lohman R, Hoang HN, Nielsen DS, Scully CCG, Kok WM, Liu L, Lucke AJ, Stoermer MJ, Schroeder CI, Chaousis S, Colless B, Bernhardt PV, Edmonds DJ, Griffith DA, Rotter CJ, Ruggeri RB, Price DA, Liras S, Craik DJ, Fairlie DP (2014) Cyclic penta- and hexaleucine peptides without N-methylation are orally absorbed. ACS Med Chem Lett. doi:10.1021/ml5002823

Hoveyda HR, Marsault E, Gagnon R, Mathieu AP, Vézina M, Landry A, Wang Z, Benakli K, Beaubien S, Saint-Louis C, Brassard M, Pinault J, Ouellet L, Bhat S, Ramaseshan M, Peng X, Foucher L, Beauchemin S, Bhérer P, Veber DF, Peterson ML, Fraser GL (2011) Optimization of the potency and pharmacokinetic properties of a macrocyclic ghrelin receptor agonist (Part I): development of Ulimorelin (TZP-101) from hit to clinic. J Med Chem 54:8305–8320

Hutchinson EG, Thornton JM (1994) A revised set of potentials for beta-turn formation in proteins. Protein Sci 3(12):2207–2216

Kabsch W, Sander C (1983) Dictionary of protein secondary structure: pattern recognition of hydrogen-bonded and geometrical features. Biopolymers 22(12):2577–2637

Karplus M (1959) Contact electron-spin coupling of nuclear magnetic moments. J Chem Phys 30(1):11–15

Kenichiro I, Passioura T, Suga H (2013) Technologies for the synthesis of mRNA-encoding libraries and discovery of bioactive natural product-inspired non-traditional macrocyclic peptides. Molecules 18:3502–3528

Knipp GT, Vander Velde GD, Siahaan TJ, Borchardt RT (1997) The effect of β-turn structure on the passive diffusion of peptides across Caco-2 cell monolayers. Pharm Res 14:1332–1340

Liu X, Wright M, Hop CECA (2014) Rational use of plasma protein and tissue binding data in drug design. Miniperspective. J Med Chem 57(20):8238–8248

Ma P, Wang Y, Van Der Hoek J, Nedelman J, Schran H, Tran LL, Lamberts SW (2005) Pharmacokinetic-pharmacodynamic comparison of a novel multi ligand somatostatin analog, SOM230, with octreotide in patients with acromegaly. Clin Pharmacol Ther 78(1):69–80

Marzinzik AL, Vorherr Th (2013) Towards intracellular delivery of peptides. Chimia 67(12):899–905

Miranda E, Nordgren IK, Male AL, Lawrence CE, Hoakwie F, Cuda F, Court W, Fox KR, Townsend PA, Packham GK, Eccles SA, Tavassoli A (2013) A cyclic peptide inhibitor of HIF-1 heterodimerization that inhibits hypoxia signaling in cancer cells. J Am Chem Soc 135(28):10418–10425

Mönkärea J, Hakalab RA, Kovalainena M, Korhonenb H, Herzigc K, Seppäläb JV, Järvinena K (2012) Photocrosslinked poly(ester anhydride)s for peptide delivery: effect of oligomer hydrophobicity on PYY3-36 delivery. Eur J Pharm Biopharm 80(1):33–38

Nielsen DS, Hoang HN, Lohman R, Diness F, Fairlie DP (2012) Total synthesis, structure, and oral absorption of a thiazole cyclic peptide, sanguinamide A. Org Lett 14(22):5720–5723

Okumu FW, Pauletti GM, Vander Velde GD, Siahaan TJ, Borchardt RT (1997) Effect of restricted conformational flexibility on the permeation of model hexapeptides across Caco-2 cell monolayers. Pharm Res 14:169–175

Over B, McCarren P, Artursson P, Foley M, Giordanetto F, Grönberg G, Hilgendorf C, Lee MD, Matsson P, Muncipinto G, Pellisson M, Perry MWD, Svensson R, Duvall JR, Kihlberg J (2014) Impact of stereospecific intramolecular hydrogen bonding on cell permeability and physicochemical properties. J Med Chem 57:2746–2754

Poillot C, Bichraoui H, Tisseyre C, Bahemberae E, Andreotti N, Sabatier J, Ronjat M, De Waard M (2012) Small efficient cell-penetrating peptides derived from scorpion toxin maurocalcine. J Biol Chem 287(21):17331–17342

Rafi SB, Hearn BR, Vedantham P, Jacobson MP, Renslo AR (2012) Predicting and improving the membrane permeability of peptidic small molecules. J Med Chem 55(7):3163–3169

Ramachandran GN, Ramakrishnan C, Sasisekharan V (1963) Stereochemistry of polypeptide chain configurations. J Mol Biol 7(1):95–99

Rand AC, Leung SSF, Eng H, Rotter CJ, Sharma R, Kalgutkar AS, Zhang Y, Varma MV, Farley KA, Khunte B, Limberakis C, Price DA, Liras S, Mathiowetz AM, Jacobson MP, Lokey RS (2012) Optimizing PK properties of cyclic peptides: the effect of side chain substitutions on permeability and clearance. Med Chem Comm 3(10):1282–1289

Rezai T, Bock JE, Zhou MV, Kalyanaraman C, Lokey RS, Jacobson MP (2006) Conformational flexibility, internal hydrogen bonding, and passive membrane permeability: successful in silico prediction of the relative permeabilities of cyclic peptides. J Am Chem Soc 128:14073–14080

Rezai T, Bock JE, Zhou MV, Kalyanaraman C, Lokey RS, Jacobson MP (2011) On-resin N-methylation of cyclic peptides for discovery of orally bioavailable scaffolds conformational flexibility, internal hydrogen bonding, and passive membrane permeability: successful in silico prediction of the relative permeabilities of cyclic peptides. Nat Chem Biol 7:810

Richmond TJ (1984) Solvent accessible surface area and excluded volume in proteins. Analytical equations for overlapping spheres and implications for the hydrophobic effect. J Mol Biol 178(1):63–89

Schaefer M, Karplus M (1996) A comprehensive analytical treatment of continuum electrostatics. J Phys Chem B 100:1578–1599

Schaefer M, Bartels C, Karplus M (1998) Solution conformations and thermodynamics of structured peptides: molecular dynamics simulation with an implicit solvation model. J Mol Biol 284(3):835–848

Seidler J, McGovern SL, Doman TN, Shoichet BK (2003) Identification and prediction of promiscuous aggregating inhibitors among known drugs. J Med Chem 46:4477–4486

Smith D, Artursson P, Avdeef A, Di L, Ecker GF, Faller B, Houston JB, Kansy M, Kerns EH, Kramer SD, Lennernäs H, van de Waterbeemd H, Sugano K, Testa B (2014) Passive lipoidal diffusion and carrier-mediated cell uptake are both important mechanisms of membrane permeation in drug disposition. Mol Pharm 11(6):1727–1738